

SUPPORTING INFORMATION FOR PUBLICATION

PEDOT(PSS) as solid contact for ion-selective electrodes: the influence of the PEDOT(PSS) film thickness on the equilibration times.

Marcin Guzinski,¹ Jennifer M. Jarvis,¹ Felio Perez² Bradford D. Pendley,¹ Erñ Lindner^{1,†}
Roland De Marco,^{3,4,5} Gaston A. Crespo,⁶ Robert G. Acres,⁷ Raymart Walker,³ Josiah Bishop,³

1. Department of Biomedical Engineering, The University of Memphis, Memphis, TN, US
2. Material Science Lab, Integrated Microscopy Center, The University of Memphis, Memphis, TN, US
3. Faculty of Science, Health, Education and Engineering, University of the Sunshine Coast, 90 Sippy Downs Drive, Sippy Downs, Queensland 4556, Australia
4. School of Chemistry and Molecular Biosciences, The University of Queensland, Brisbane, Queensland 4072, Australia
5. Department of Chemistry, Curtin University, GPO Box U1987, Perth, Western Australia 6109, Australia
6. Department of Inorganic and Analytical Chemistry, University of Geneva, Quai Ernest-Ansermet 30, CH-1211 Geneva, Switzerland
7. Australian Synchrotron, 800 Blackburn Road, Clayton, VIC 3168, Australia

TABLE OF CONTENT

EXPERIMENTAL SECTION

- XPS surface analysis
- SR-XPS surface analysis
- Calculation of NaPSS-to-PEDOT, EDOT_n⁺ PSS⁻-to-PEDOT, and atomic ratios
- Calculation of inelastic mean free paths of photoelectrons in SR-XPS

RESULTS

- Potential vs. time transients recorded during the equilibration PEDOT(PSS)-coated Pt, Au and GC electrodes following the galvanostatic deposition of the PEDOT(PSS) films
- Potential vs. time transients recorded during equilibration of PEDOT(PSS)-coated GC electrode and of PEDOT(PSS)-based SC K⁺ ISEs with GC as substrate electrode: Influence of the PEDOT(PSS) film thickness
- SR-XPS results

REFERENCES

[†] Corresponding author, Phone: (901) 678-5641. Fax: (901) 678-5281. Email: elindner@memphis.edu

EXPERIMENTAL SECTION

XPS surface analysis

XPS analysis of the PEDOT(PSS) samples was performed using a Thermo Scientific K-Alpha XPS system equipped with a monochromatic Al K α X-ray source at 1486.6 eV. The X-ray power of 75 W at 12 kV was used for all experiments with a spot size of 400 μm^2 . The base pressure of this instrument was 10^{-9} mbar. The instrument was calibrated to give a binding energy of 84.0 eV for Au 4f $_{7/2}$ (also in SR-XPS studies) and 284.6 eV for the C1s line of adventitious (aliphatic) carbon present on the non-sputtered samples. Photoelectrons were collected from a takeoff angle of 90 $^\circ$ relative to the sample surface. The Pt, Au, and GC electrodes (BASi MF 1012, MF 1002 and MF 1000, respectively) coated with 100 nm thick electrochemically deposited PEDOT(PSS) were sputtered with an Ar $^+$ gun to perform a depth profile analysis. A series of XPS spectra at 150 etching-levels were recorded in constant analyzer energy mode. Survey spectra were taken at each level with 200 eV pass energy, while the high resolution core level spectra of C 1s, O 1s, S 2p, Na 1s, Pt 4f and Au 4f were taken at a 40 eV pass energy, an energy step size of 0.1 eV using an average of 10 scans. The XPS data acquisition was performed using the “Avantage v5.932” software provided with the instrument.

SR-XPS surface analysis

Argon ion and photon energy dependent synchrotron radiation-XPS (SR-XPS) surface analysis of electrochemically polymerized PEDOT(PSS) was performed at the Australian Synchrotron (AS) soft X-ray (SXR) beamline, while photon energy dependent SR-XPS depth profiles of ~ 10 nm thick PEDOT(PSS) films were measured at both the AS SXR beamline and the Elettra Materials Science beamline (MSB) (Elettra – Synchrotron, Trieste, Italy). Since the bending magnet Elettra MSB has a diminished beam brilliance and concomitant beam damage compared to the high flux undulator SXR beamline at the AS and may be used in the measurement of reliable valence band (VB) spectra owing to its ability to access lower photon energies of 30 eV compared to the AS SXR beamline, the Elettra MSB was the beamline of choice for this surface study of PEDOT(PSS).

Ion sputtering and beam induced damage of the PSS $^-$ species in PEDOT(PSS) is highly problematic, as illustrated in the SR-XPS results sections (Figures S5 and S6) of this supplementary Information. Consequently, photon energy dependent SR-XPS depth

profiling of thin films of PEDOT(PSS) at Elettra MSB were essential to the successful completion of this study.

SR-XPS surface analysis at Elettra – Synchrotron MSB: Valence band (VB) spectra at a photon energies from 40 eV and photon energy dependent SR-XPS depth profiling of the S 2p core level at photon energies of 220, 320, 570 and 970 eV were recorded at the MSB at the Elettra synchrotron light source in Trieste Italy. The MSB end-station comprises an ultrahigh vacuum instrument (10^{-10} mbar base pressure, and was maintained at 5×10^{-9} mbar or better during measurements) that is equipped with a Specs Phoibos 150 multichannel electron energy analyzer along with an argon gas inlet and argon ion sputtering gun.

SR-XPS at the soft X-ray (SXR) beamline at the Australian Synchrotron (AS): Synchrotron radiation-XPS (SR-XPS) survey and high resolution spectra were recorded on the Australian Synchrotron (AS) soft X-ray (SXR) beamline in Melbourne, Australia. High-resolution S 2p spectra were recorded at photon energies of 220, 320, 570, 970, and 1487 eV, and all measurements were performed at an angle of 55° with respect to the sample normal. This beamline utilizes an insertion device based on an elliptically polarized undulator providing a flux between 5×10^{11} and 3×10^{12} photons/200 mA at the sample at 400 eV. The optimal energy range of the beamline is between 90 to 2000 eV with a resolution ($E/\Delta E$) of 5,000 to 10,000 and beam size of 0.6 mm \times 0.6 mm. The end-station was constructed by OmniVac and PreVac using a SPECS Phobios 150 hemispherical electron energy analyzer in conjunction with photodiode and drain current detectors. The analyzer chamber was maintained at 1×10^{-9} mbar or lower and the storage ring was operated in the decay mode.

Ion sputtering beam-induced damage of the PEDOT(PSS) film on Au was ascertained by sputtering the sample for 90 s (or a depth of 5.5 nm) at 600 V, 5 mA and 5×10^{-6} mbar of Ar, noting that the sputter rate of this ion gun was previously found to be 3.7 ± 0.4 nm/min¹.

CasaXPS was used to fit Gaussian/Lorentzian peaks together with a Shirley background correction, so as to deconvolute spectra comprising multiple components. Since the effect of photon energy on the Scofield photoabsorption cross-section and asymmetry parameter of the S 2p orbital together with the influence of electron kinetic energy on the spectrometer transmission function and inelastic mean free path of the photoelectrons are similar on both the PEDOT and PSS components in the S 2p spectra, the ratio of PSS-to-PEDOT peak intensities is equivalent to the mole ratio of PSS-to-PEDOT.

Calculation of NaPSS-to-PEDOT, $EDOT_n^+PSS^-$ -to-PEDOT, and atomic ratios

PSS^- (PSS_{tot}) can be incorporated into the electrochemically deposited PEDOT(PSS) film as Na^+PSS^- and as $EDOT_n^+PSS^-$, i.e., $PSS_{tot} = Na^+PSS^- + EDOT_n^+PSS^-$. For approximately 10 nm thick PEDOT(PSS) films (see Figure 4 in the manuscript), the averages in $PSS_{tot}/PEDOT$ ratios have been determined to be 1.16, 0.97 and 0.24 on Pt, GC, and Au substrate electrodes, respectively. Since the Elettra Materials Science Beamline (MSB) can only achieve a maximum beam energy of 1000 eV, it was not possible to access the Na 1s core orbital at about 1072 eV for NaPSS on these samples at Elettra. Consequently, we electropolymerized approximately 10 nm thick films of PEDOT(PSS) onto the same electrode substrates utilizing identical electropolymerization conditions to those used at Elettra, and analyzed these samples using laboratory XPS. These multiple spot analyses yielded Na^+/PSS_{tot} ratios (average of 3 spot analyses on each film) of 0.7, 0.2, and 0.8 on Pt, GC, and Au, respectively. The methodology used in the deduction of $Na^+PSS^-/PEDOT$, $EDOT_n^+/PEDOT$, and $EDOT_n^+/EDOT_m^0$ ratios in Table 3 of the main manuscript is shown through the calculation for Pt electrode:

$$\frac{NaPSS}{PEDOT} = \frac{Na^+}{PSS_{tot}} \times \frac{PSS_{tot}}{PEDOT} = 0.7 \times 1.16 = 0.81 \text{ or } 81\text{mol}\% (Pt) \quad (S1)$$

$$EDOT_n^+ = PSS_{tot} - Na^+PSS^- \quad (S2)$$

$$\frac{EDOT_n^+}{PEDOT} = \frac{PSS_{tot}}{PEDOT} - \frac{Na^+PSS^-}{PEDOT} = 1.16 - 0.81 = 0.35 \text{ or } 35 \text{ mol}\% (Pt) \quad (S3)$$

$$EDOT_n^+ + EDOT_m^0 = PEDOT \quad (S4)$$

$$\frac{EDOT_m^0}{PEDOT} = 1 - \frac{EDOT_n^+}{PEDOT} = 1 - 0.35 = 0.65 (Pt) \quad (S5)$$

$$EDOT_n^+/EDOT_m^0 = \frac{0.35}{0.65} = 0.54 (Pt) \quad (S6)$$

Calculation of inelastic mean free paths of photoelectrons in SR-XPS

The inelastic mean free paths, IMFPs, of organic soft matter, which is representative of the PEDOT(PSS) films investigated in this study, are given by:

$$IMFP_i = 49 \left(\frac{1}{(E_k)^2} \right) + 0.11\sqrt{E_k} \quad (S7)$$

where E_k is kinetic energy of the photoelectrons in eV from the core level atomic orbital.

Since the binding energies of the PEDOT and PSS⁻ S 2p components of the SR-XPS spectra differ by a small amount (viz., a few eV), we have utilized the mid-point binding energy of 166 eV in calculations of the IMFPs at the photon energies utilized in the SR-XPS photon energy dependent depth profiling experiments (see Table S1).

Table S1. IMFPs as a function of photon energy calculated using Equation S7 together with an average S 2p binding energy of 166 eV for the PEDOT and PSS⁻ components at approximately 164 and 168 eV respectively.

Photon energy / eV	220	320	570	970	1487
Kinetic energy / eV	54	154	404	804	1321
IMFP / nm	0.83	1.37	2.21	3.12	4.00

RESULTS

Potential vs. time transients recorded during the equilibration PEDOT(PSS)-coated Pt, Au and GC electrodes following the galvanostatic deposition of the PEDOT(PSS) films

To follow changes in the redox state of the galvanostatically deposited PEDOT(PSS) films as function of time the potentials of PEDOT(PSS)-coated Pt, Au, and GC electrodes were recorded for 24 hours immediately after completing the galvanostatic deposition of 1.0 μm or 0.1 μm thick PEDOT(PSS)-films. The potential vs. time transients shown in Figure S1 were recorded with 1.0 μm thick PEDOT(PSS)-coating in the same solution which has been used for the PEDOT(PSS) deposition (0.015 mol/dm³ EDOT and 0.1 mol/dm³ NaPSS). The shapes of the transients were very similar when the PEDOT(PSS)-coating over the Pt, Au, and GC electrode was only 0.1 μm thick but the rates were higher and the potential values measured at the end of the experiment (after 24 hours of equilibration) were more positive (52 mV, 55 mV and 26 mV for Pt, Au, and GC electrodes, respectively) than with the 1.0 μm thick PEDOT(PSS)-coated electrodes. However, the significant differences between the Pt and Au and GC electrodes remained.

The complexity of the interpretation of the equilibration processes is easily understood by considering the potential vs. time traces of the PEDOT(PSS)-coated Pt electrode. As shown in the figure S1 after about 5.2 ± 0.4 (n=3) hours of equilibration the drift abruptly changes sign (from negative to positive) without any change in the composition of the solution, temperature etc. With 0.1 μm thick PEDOT(PSS)-coating on the electrodes the change in the sign of the drift becomes visible with all three electrodes but

the time instant when it happens is very different 3.6 ± 0.1 (n=4) hours with Pt, 8 ± 4 (n=3) hours with Au, and 14.4 ± 2.6 (n=5) hours with GC electrodes.

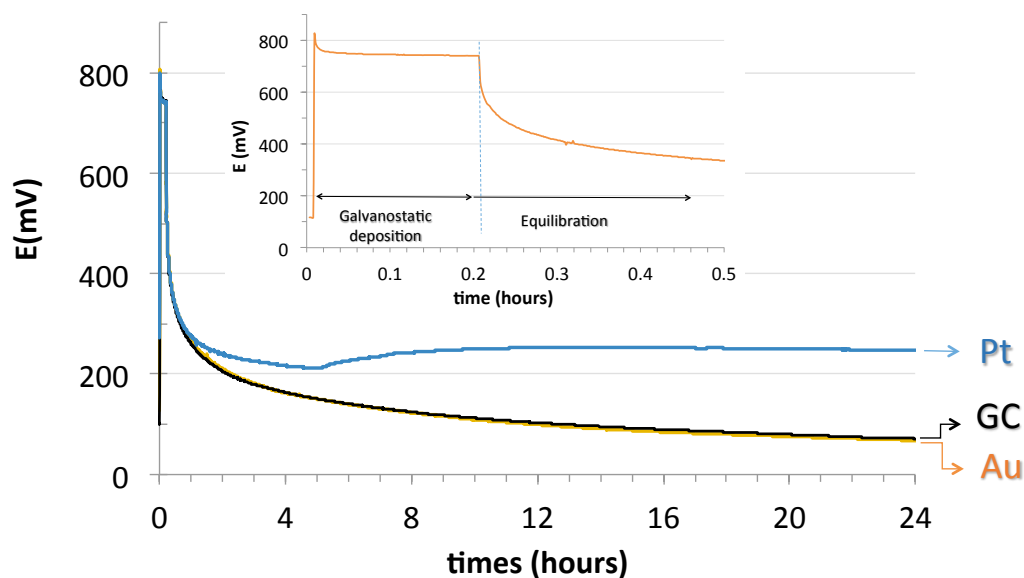


Figure S1: Potential vs. time transients recorded at two different time scales during the galvanostatic deposition (0-0.2 hours, inset) and consecutive equilibration (0.2-24 hours) of PEDOT(PSS)-coated Pt, GC and Au electrodes in the solution used to for the electrochemical deposition) (0.015 mol/dm^3 EDOT and 0.1 mol/dm^3 NaPSS). The layer thickness of the PEDOT(PSS) film was $1.0 \mu\text{m}$ for all three electrodes.

Potential vs. time transients recorded during equilibration of PEDOT(PSS)-coated GC electrode and of PEDOT(PSS)-based SC K^+ ISEs with GC as substrate electrode: Influence of the PEDOT(PSS) film thickness

Figures S2 shows the potential vs. time transients recorded in 0.1 M KCl with PEDOT(PSS)-coated GC electrodes and PEDOT(PSS)-based SC ISEs fabricated with 0.1 , 1.0 , 2.0 , and $4.0 \mu\text{m}$ PEDOT(PSS) thicknesses on GC substrate electrodes, respectively. These transients are shown to demonstrate the similarities between the equilibration properties of PEDOT(PSS)-coated GC and Au electrodes (compare Figures 2a with S2a) as well as between PEDOT(PSS)-based SC ISEs fabricated on GC and Au substrate electrodes (compare Figures 2b with S2b).

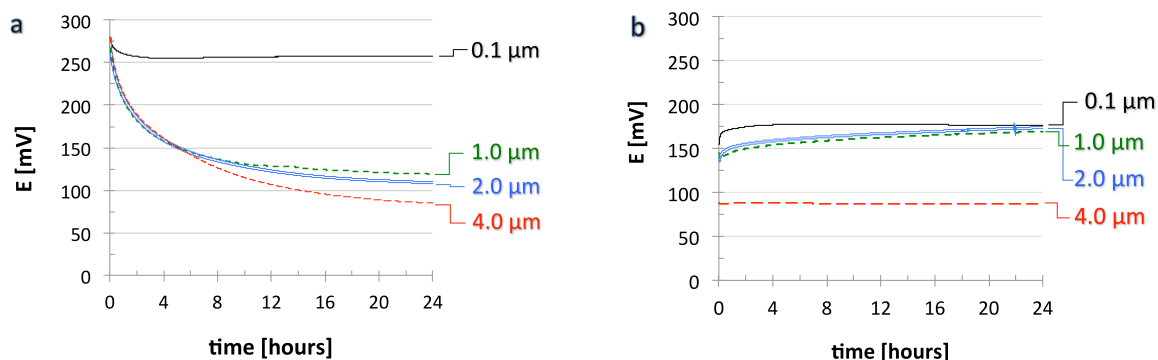


Figure S2: Potential vs. time transients recorded during the equilibration of PEDOT(PSS)-coated GC electrodes (a) and fully fabricated potassium-selective electrodes prepared on GC with PEDOT(PSS) as solid contact (b) in 0.1M KCl. The PEDOT(PSS) films (0.1 μm , 1.0 μm , 2.0 μm , and 4.0 μm) were deposited onto the GC electrodes electrochemically.

SR-XPS results

Figures S3 and S4 present the S 2p and O 1s SR-XPS spectra of the native PEDOT(PSS) surface after electropolymerization onto Au, as measured at the SXR beamline in Australia. The presence of a pair of S 2p_{3/2} and S 2p_{1/2} spin-orbit split component peaks at 163.7 and 164.9 eV together with 168.1 and 169.3 eV (see Figure S3) are consistent with sulfur in the PEDOT backbone of PEDOT(PSS) and the sulfonate functionality of the PSS⁻ counteranion.²

Similarly, the presence of an O 1s peak at 533.2 eV is symbolic of oxygen in the ethoxy functionality of the PEDOT backbone, while the peak at 531.6 eV is ascribable to oxygen in the sulfonate functionality of the PSS⁻ counteranion² (see Figure S4). Note that the small pair of S 2p_{3/2} and S 2p_{1/2} spin-orbit split peaks at 165.0 and 166.2 eV are indicative of the PEDOT⁺ polaron in oxidized PEDOT. From the S 2p spectra (Figure S3), it is evident that the ratio of PSS_{tot}⁻ to-PEDOT on Au is about 0.25, or 25%.

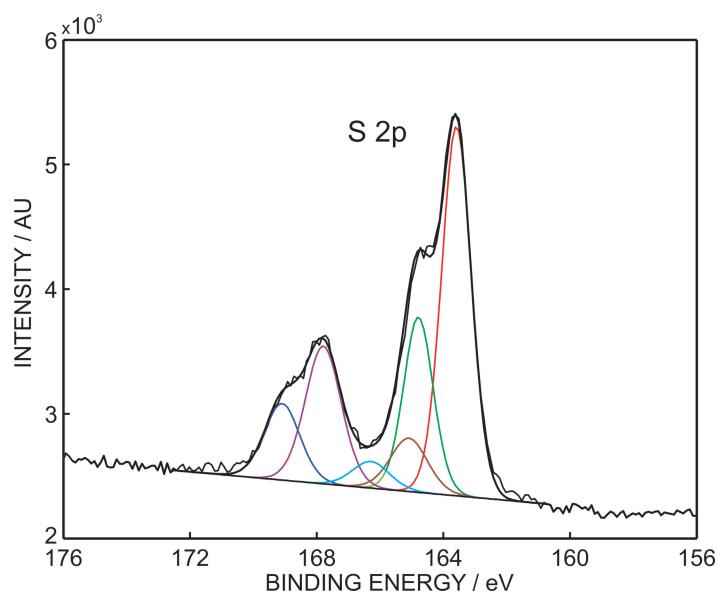


Figure S3. SR-XPS spectrum of the S 2p core level for electropolymerized PEDOT(PSS) on Au (approximate 10 nm film thickness) as measured on the SXR beamline at the Australian Synchrotron.

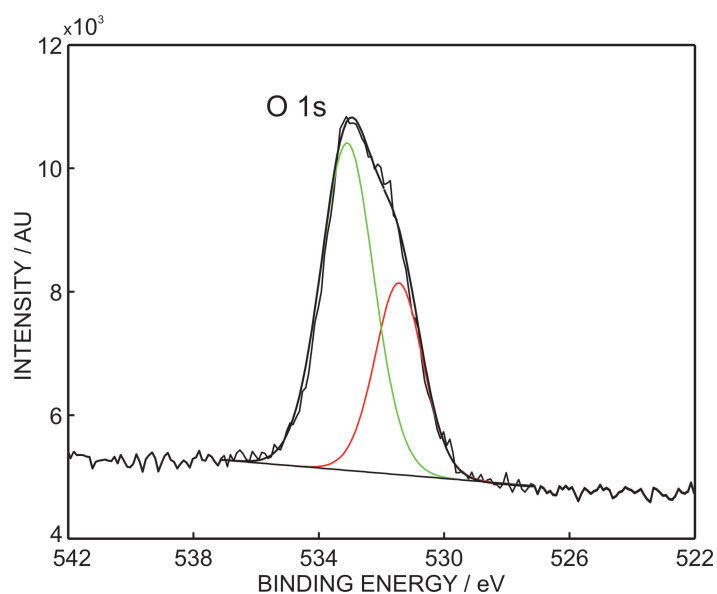


Figure S4. SR-XPS spectrum of the O 1s core level for electropolymerized PEDOT(PSS) on Au (approximate 10 nm film thickness) as measured on the SXR beamline at the Australian Synchrotron.

We also undertook Ar ion sputtering of PEDOT(PSS) electropolymerized onto Au to the middle of the film (see Figure S5 for the corresponding S 2p spectra of unsputtered and sputtered surfaces), so as to ascertain if there was ion beam induced damage of the PEDOT(PSS). It is obvious that Ar ion sputtering has preferentially sputtered/damaged the PSS⁻ component of PEDOT(PSS) at about 168 eV, as has been illustrated elsewhere,³ and the

presence of a small shoulder at about 162 eV is symbolic of elemental sulfur that has been formed by sulfur reduction in the ion beam. This ion beam induced damage provided the motivation for this surface study of PEDOT(PSS) using a non-destructive photon energy dependent depth profiling of PEDOT(PSS) at a synchrotron light source.

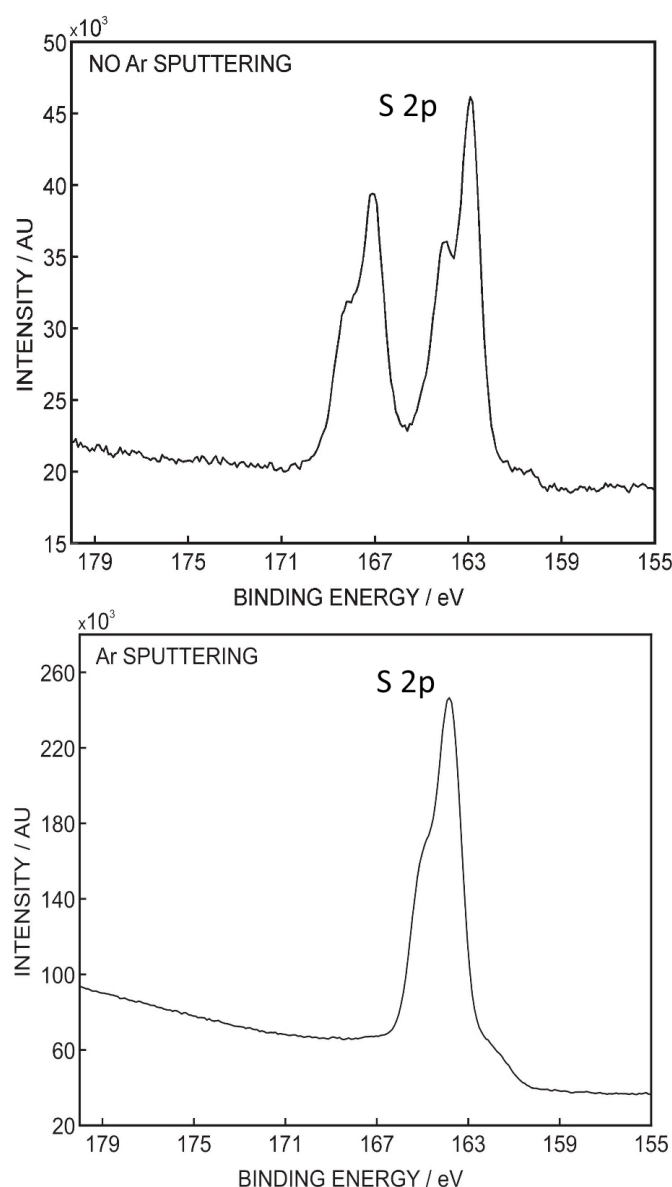


Figure S5. SR-XPS S 2p spectrum on an Au substrate (approximate 100 nm film thickness) before and after Ar ion sputtering to a depth of approximately 5.5 nm measured at the Australian Synchrotron SXR beamline.

A photon energy dependent depth profiling of the thin PEDOT(PSS) films yielded very similar results on the undulator SXR beamline at the AS (see Figure S6) to those shown in Figure 4 of the main manuscript which were measured at the Elettra MSB in Italy with low PSS⁻-to-PEDOT ratios on Au and markedly higher on GC and Pt. It is significant to note that

the photon energy dependent studies involved an initial SR-XPS analysis at a photon energy of 200 or 1487 eV, with subsequent analyses at the higher or lower photon energies on the same analysis spot. The results shown in Figure S6 indicate that the high brilliance undulator SXR beamline has damaged the samples. This is the reason why the Elettra MSB was the instrument of choice in this study.

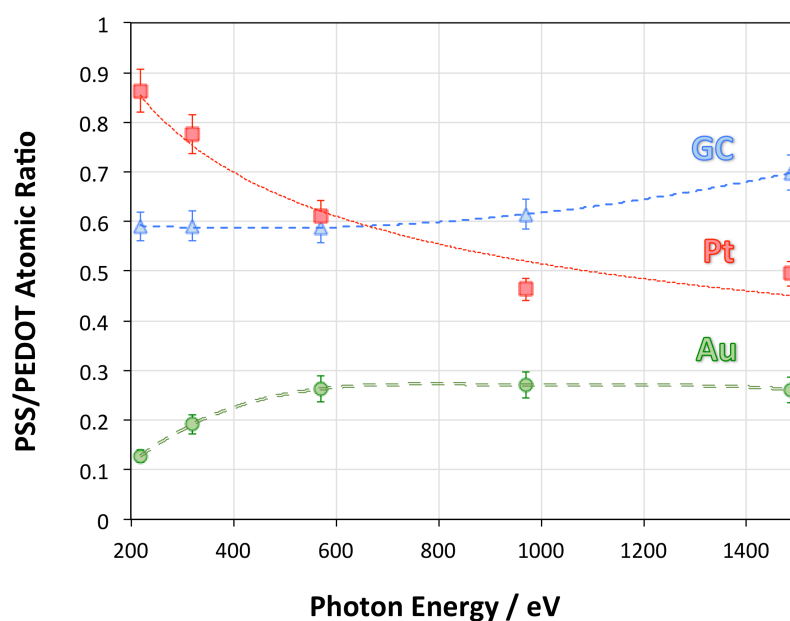


Figure S6. SR-XPS PSS⁻-to-PEDOT ratios measured at the AS SXR beamline for approximately 10 nm thick PEDOT(PSS) films electropolymerized on Au, GC, and Pt .

Figure S7 presents the valence band (VB) spectra for PEDOT(PSS) electropolymerized onto Au, Pt, and GC, noting that SR-XPS showed that Au only had about a 24% level of doping by PSS⁻, while GC had about a 100% doping and Pt showed an approximate 120% level of doping by PSS⁻ (see Figure 4 in the main manuscript). It is evident that the much lower density of states (DOS) with less doped PEDOT formed on Au versus Pt and GC is consistent with a change in the band structure and the concomitant electrical conductivity of less oxidized and doped PEDOT(PSS) on Au versus more oxidized and doped PEDOT(PSS) on GC and Pt. The small peaks in Figure S7 at about 13 and 17 eV are due to the C 2s orbital,⁴ while the major peaks at about 8.7, 6.2 eV, and the unresolved bump at about 4 eV are related to the σ and π hybrid states among O 2p, C 2p and S 3p orbitals.⁴ A comparative absence of the unresolved bump at about 4 eV (highest occupied molecular orbital or HOMO) on Au is indicative of an absence of PSSH and DOS related to the p-type PEDOT associated with pure EDOT_n⁺ PSS⁻,⁴ which is expected given that this sample is only partially

oxidized and doped. Notably, the abrupt decrease in DOS below 1.5-2.5 eV with the PEDOT films (see Figure S8) together with a smooth tail to the Fermi level at 0 eV is associated with electrons due to the presence of localized filled states from the disordered or PEDOT(PSS) Fermi glass.⁵

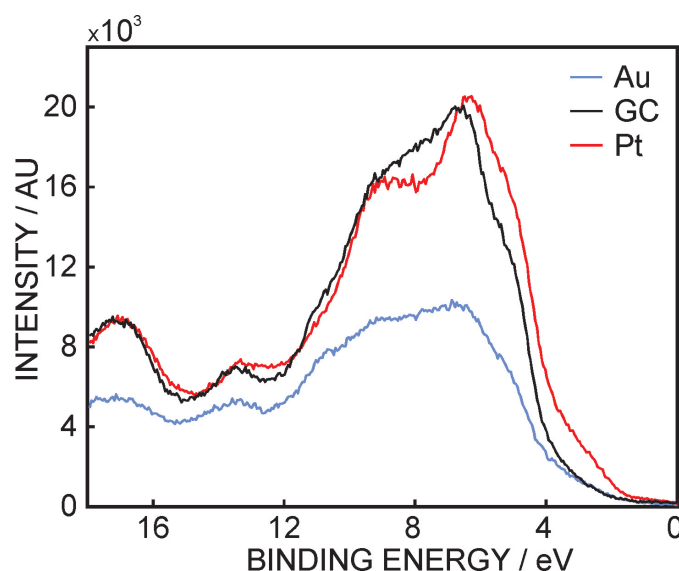


Figure S7. VB spectra for approximately 10 nm thick PEDOT(PSS) films electropolymerized onto Au, GC, and Pt as electrode substrates and recorded using a photon energy of 74 eV.

Figure S8 shows the DOS from the Fermi level to a few eV, and there are obvious differences between the energies of the Fermi level and VB maximum, or ($E_{\text{VBM}} - E_{\text{F}}$), as a function of substrate, noting that the GC and Au samples have comparable NaPSS levels of 19 mol% against PEDOT, while the Pt sample has a considerably higher level of NaPSS (about 81 mol% against PEDOT) corresponding to a substantially increased hydrophilicity of the PEDOT(PSS) film on Pt vs GC and Au. This is a significant point since Miller et al.⁶ illustrated that the values of ($E_{\text{VBM}} - E_{\text{F}}$) for $\text{CH}_3\text{NH}_3\text{PbI}_3$ on various substrates can vary by about 0.5 eV depending on exposure to moisture, so this difference is most likely ascribable to water sorption in the PEDOT(PSS) films. Nevertheless, the slopes of the DOS from near to the Fermi level to a few eV, which are symbolic of the Seebeck coefficients or thermoelectric power factors of these PEDOT films,⁵ demonstrate as expected that there are higher rates of charge carrier diffusion in the more oxidized and doped PEDOT(PSS) films on Pt and GC (also comparable) as opposed to a much lower value in the 24% total PSS-doped PEDOT(PSS) film (comprising $\text{EDOT}_n^+ \text{PSS}^- / \text{PEDOT} \approx 0.05$) that was formed on Au.

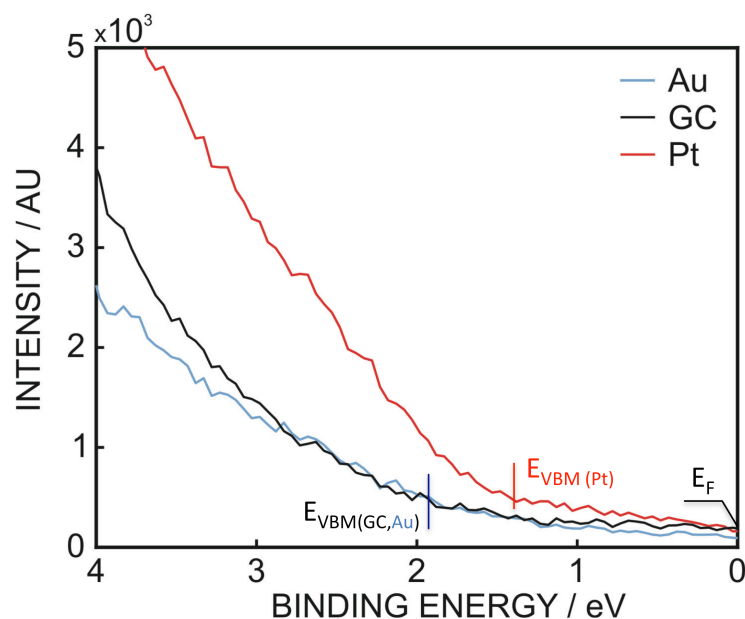


Figure S8. Expanded plots of density of states (DOS) versus energy near to the Fermi edge in Figure S7, so as to elucidate trends in the Seebeck coefficients for thermoelectric conduction in the PEDOT(PSS) films.

REFERENCES

- (1) Seah, M.P.; Dench, W.A., *Surf. Interface Anal.* **1979**, *1*, 2-11.
- (2) Greczynski, G.; Kugler, T.; Keil, M.; Osikowicz, W.; Fahlman, M.; Salaneck, W.R. *J. Electron Spectrosc. Relat. Phenom.* **2001**, *121*, 1-17.
- (3) Hwang, J.; Amy, F.; Kahn, A. *Org. Electron.* **2006**, *7*, 387-396.
- (4) Yun, D.J.; Ra, H.; Kim, J.; Hwang, I.; Lee, J.; Rhee, S.W.; Chung, J.G. *ECS J. Solid State Sci. Technol.* **2012**, *1*, M10-M14.
- (5) Bubnova, O.; Khan, Z.U.; Wang, H.; Braun, S.; Evans, D.R.; Fabretto, M.; Hojati-Talemi, P.; Dagnelund, D.; Arlin, J.B.; Geerts, Y.H.; Desbief, S.; Breiby, D.W.; Andreasen, J.W.; Lazzaroni, R.; Chen, W.M.; Zozoulenko, I.; Fahlman, M.; Murphy, P.J.; Berggren M.; Crispin, X. *Nature Mater.* **2014**, *13*, 190-194.
- (6) Miller, E.M.; Zhao, Y.; Mercado, C.C.; Saha, S.K.; Luther, J.M.; Zhu, K.; Stevanovic, V.; Perkins, C.L.; van de Lagemaat, J. *Phys. Chem. Chem. Phys.* **2014**, *16*, 22122-22130.